ACS APPLIED MATERIALS & INTERFACES

Research Article

www.acsami.org

Biofunctionalization of α-Zirconium Phosphate Nanosheets: Toward Rational Control of Enzyme Loading, Affinities, Activities and Structure Retention

Inoka K. Deshapriya,[†] Christina S. Kim,[†] Marc J. Novak,[†,‡] and Challa V. Kumar*[,†,‡]

[†]Department of Chemistry, [‡]Department of Molecular and Cell Biology, University of Connecticut, Storrs, Connecticut 06269, United States

Supporting Information

ABSTRACT: Controlling the properties of enzymes bound to solid surfaces in a rational manner is a grand challenge. Here we show that preadsorption of cationized bovine serum albumin (cBSA) to α-Zr(IV) phosphate (α-ZrP) nanosheets promotes enzyme binding in a predictable manner, and surprisingly, the enzyme binding is linearly proportional to the number of residues present in the enzyme or its volume, providing a powerful, new predictable tool. The cBSA loaded α-ZrP (denoted as bZrP) was tested for the binding of pepsin, glucose oxidase (GOX), tyrosinase, catalase, myoglobin and laccase where the number of residues increased from the lowest value of ∼153 to the highest value of 2024. Loading depended linearly on the number of residues, rather than enzyme charge or its isoelectric point. No such correlation was seen for the binding of these enzymes to α-ZrP nanosheets without the preadsorption of cBSA, under similar conditions of pH and buffer. Enzyme binding to bZrP was supported by centrifugation studies, powder X-ray diffraction and scanning electron microscopy/energy-dispersive X-ray spectroscopy. All the bound enzymes retained their secondary structure and the extent of structure retention depended directly on the amount of cBSA preadsorbed on α-ZrP, prior to enzyme loading. Except for tyrosinase, all enzyme/bZrP biocatalysts retained their enzymatic activities nearly 90−100%, and biofunctionalization enhanced the loading, improved structure retention and supported higher enzymatic activities. This approach of using a chemically modified protein to serve as a glue, with a predictable affinity/loading of the enzymes, could be useful to rationally control enzyme binding for applications in advanced biocatalysis and biomedical applications.

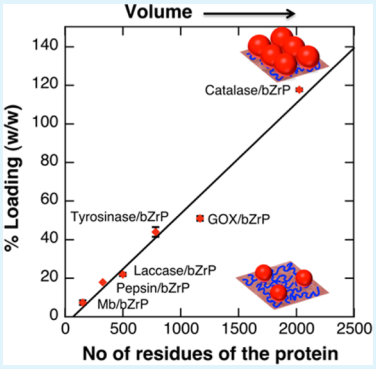

KEYWORDS: *α-ZrP, bZrP, nanomaterials, cationization, protein-o-philic, intercalation*

INTRODUCTION

Inorganic nanomaterials provide excellent platforms for enzyme binding with a high degree of structure and activity retention with improved stability.[1−4] Here we show that preadsorption of cationized bovine serum albumin (cBSA) onto the anionic nanosheets of α-zirconium phosphate ($(\alpha\text{-}Zr(HPO_4)_2)$), denoted as α-ZrP provided an excellent control over enzyme binding to the solid. α-ZrP is a highly hydrated, anionic, inert, lamellar material with a high surface area (100 m^2/g),[5] and α-ZrP provides a benign environment for favorable binding of positively charged biomolecules.[6] Enzymes intercalated in the galleries of α-ZrP indicated high stabilities and excellent activity retention (60−140%).[4] The phosphate lattice of α-ZrP nanosheets provides a uniform, hydrated, charged surfaces for interactions with positively charged enzymes and proteins.[7] However, the strong negative charge field of α-ZrP severely limits the binding of strongly negatively charged biomolecules due to the unfavorable electrostatic repulsions.

Several methods were tested to overcome this electrostatic barrier by tuning the surface charge of the solid via the preadsorption of metal ions, for example, which served as metal glues for enzyme binding.[8] However, the use of metal ions to promote binding of anionic enzymes to anionic solid surfaces has an intrinsic risk of inhibiting particular enzymes or deactivating them by the added metal ion.[9,10]

In another approach, the COOH residues of negatively charged proteins were modified with polyamines to reverse their net charge.[11] Enzyme cationization, via the polyamine modification, strongly promoted binding by several orders of magnitude.[8] Chemical modification of enzymes, however, could be deleterious to the sensitive structures of certain enzymes and it may not be a practical approach when the enzyme samples are available only in limited quantities or they do not have a sufficient number of accessible sites for the modification. Alternative, but simpler and universally applicable, systematic approaches to induce high affinity binding of anionic enzymes to anionic solids, therefore, will be useful.

In this context, we considered coating α-ZrP with a suitable protein glue such that the glue binds to both the solid and the enzyme with high affinities, as an alternative to enzyme

Received: April 4, 2014
Accepted: May 22, 2014
Published: May 22, 2014

 © 2014 American Chemical Society

Scheme 1. (A) Schematic Representation of Biofunctionalization of α-ZrP with Cationized BSA (BSA-TETA(+27)), Followed by the Binding of Negatively Charged Proteins. (B) Distribution of Anionic (red) and Cationic (blue) Residues on the Five Enzymes Examined Here, and Their Respective Isoelectric Points (pI), Molecular Weights, Surface Area and the Charge Per Unit Area

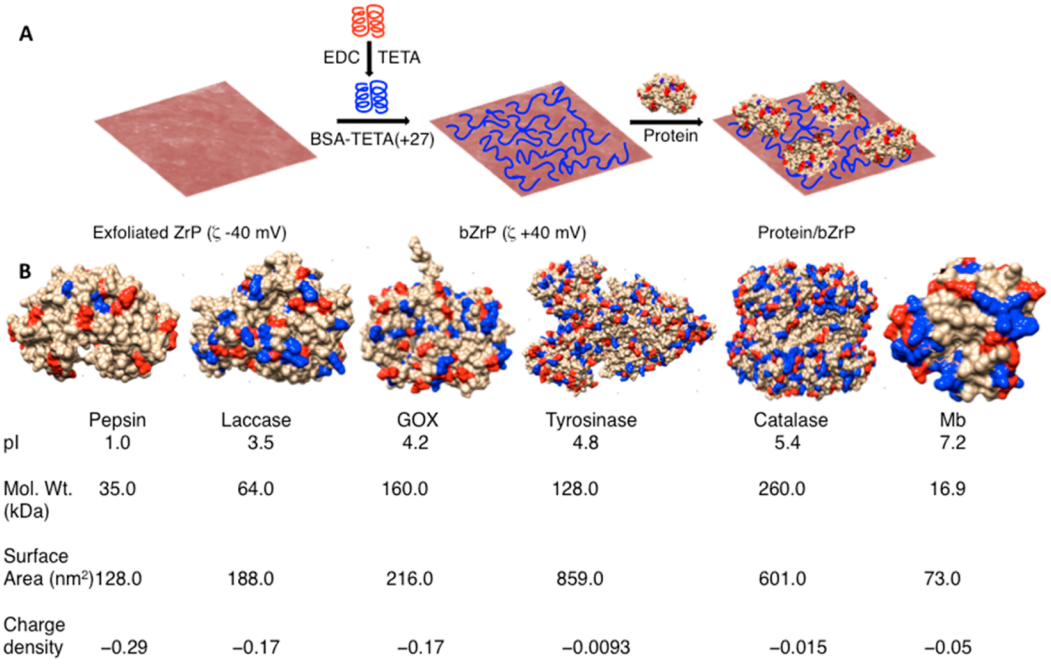

	Pepsin	Laccase	GOX	Tyrosinase	Catalase	Mb
pI	1.0	3.5	4.2	4.8	5.4	7.2
Mol. Wt. (kDa)	35.0	64.0	160.0	128.0	260.0	16.9
Surface Area (nm^2)	128.0	188.0	216.0	859.0	601.0	73.0
Charge density	−0.29	−0.17	−0.17	−0.0093	−0.015	−0.05

chemical modification (Scheme 1). Our approach is 2-fold: (1) control the charge of α-ZrP nanosheets by the preadsorption of a sacrificial, cationized protein and (2) passivate high energy sites on α-ZrP surface for a high retention of bound enzyme structure and activities.

A cationic glue-coated surface could offer a robust platform to predict the binding affinities of a number of acidic proteins to anionic surfaces, as the interactions between the side chains of the glue and that of the bound enzyme are more likely to be governed by protein−protein interactions rather than protein−solid interactions.

This approach is tested here by using cationized bovine serum albumin (cBSA) as the artificial protein glue and α-ZrP as a model solid (Scheme 1). BSA is an abundant, water-soluble, inexpensive, serum protein with a molecular weight of 66 000 Da, and it is commonly used to prevent cell adhesion to plastic culture media.[12] BSA adsorbs to various nonbiological surfaces and modifies their biodurability and biopersistence.[13] For instance, BSA was used to convert graphene oxide to reduced graphene,[14] and BSA adsorption to solids proceeds via electrostatic[15−17] and/or hydrophobic interactions.[18] The low isoelectric point of BSA (pI, 4.6)[19] renders it negatively charged at pH 7, a desirable pH for biological applications. But, it has a very weak affinity for the anionic nanosheets of α-ZrP. However, cationization would enhance the affinity of the modified BSA (cBSA) to anionic solid surfaces as well as acidic proteins and could serve as a potential protein glue.

BSA has been cationized in our laboratories by amidation of its COOH groups with triethylenetetraamine (TETA) using carbodiimide chemistry (Scheme 1).[20] The high positive charge of cBSA favored its binding to negatively charged DNA[21] and in the current studies, we tested the use of cBSA as a natural adhesive for the favorable binding of strongly anionic proteins to anionic α-ZrP.

Moreover, BSA has a low structural stability[22] and it tends to denature upon binding to many solid surfaces.[23,24] This aspect of BSA was also exploited here to bind and cover the surface of α-ZrP, where cBSA could be spread across the solid surface, covering the phosphate groups of the solid with a variety of amino acid side chains. The charge of the biofunctionalized cBSA/α-ZrP (bZrP) can be controlled by the amount of cBSA loaded on the solid, as well as by controlling the net charge of cBSA.

Previously, we showed that cBSA could be used to control the binding of enzymes to the hydrophobic nanosheets of graphene oxide (GO). While the extent of structure and activity retention of the bound enzymes improved substantially, enzyme loading on the nanosupport did not respond well.[25] One explanation was that bare GO binds enzymes via hydrophobic interactions, and blocking these sites with cBSA improved structure/activity retention but not loading. Here, we tested this explanation using the strongly anionic, hydrated, ionic surfaces of α-ZrP with negatively charged enzymes to promote their binding and activity retention with bZrP.

A small set of anionic enzymes (pepsin (pI 1[26]), laccase (pI 3.5[27]), glucose oxidase (GOX, pI 4.2),[28] tyrosinase (pI 4.8[29]), catalase (pI, 5.4) and myoglobin (pI 6.9)[4] with increasing sizes, surface charges (Scheme 1), isoelectric points and different catalytic activities are tested for their binding to bZrP. Pepsin is a strongly negatively charged proteolytic enzyme used in peptide synthesis, but it has little or no affinity for anionic α-ZrP. GOX is an oxido-reductase,[30] which catalyzes the oxidation of glucose by ambient oxygen, and GOX is highly promising for biosensor and biofuel cell applications.[31] Encapsulation of GOX in a solid can improve its stability, reusability and could improve its practical applications, but GOX binds very poorly to α-ZrP.[7,32] Laccase and tyrosinase are Cu-containing oxidases, which catalyze the oxidation of phenols and polyphenols while reducing dioxygen to water, and they are

potentially interesting for biofuel cell applications.[33] Several metal ions such as Fe^{2+}, Co^{2+}, Mn^{2+}, Na^{+} and K^{+} inhibit laccase activity[34] and such ions could not be used to enhance the affinity of laccase for α-ZrP. Similarly, Cu^{2+} and Mn^{2+} inhibit tyrosinase affinity.[35] Therefore, using metal ions to promote the binding of these anionic enzymes to anionic solids is not an attractive proposition. Catalase is another anionic enzyme of practical importance, it decomposes hydrogen peroxide to water and oxygen, under ambient conditions, and plays a key biological role in neutralizing reactive oxygen species in cells, greying of hair and protecting the cell from oxidative damage.[36]

Therefore, the enzymes selected here have potential practical applications and also provide a spectrum of physical/biological properties. Current investigations show that cBSA provided a rational control of enzyme loading on α-ZrP; the extent of structure retention also depended linearly on cBSA loading, and the enzyme loading scaled linearly with the number of residues present in the enzyme, rather than its charge. Thus, biofunctionalization of α-ZrP with cBSA is an important step in controlling the enzyme−solid interface in a rational, predictable manner.

MATERIALS AND METHODS

Materials. Triethylenetetraamine (TETA), Guaiacol, Syringaldazine, Laccase, Pepsin A, GOX, catalase and bovine serum albumin (BSA) were purchased from Sigma-Aldrich (St. Louis, MO). Peroxidase type 1 from horseradish (HRP; specific activity of 356 U/mg) and tyrosinase were purchased from Calzyme Laboratories (San Luis Obispo, CA) and Worthington Biomedical Corporation (Lakewood, NJ), respectively.

Synthesis of BSA-TETA(+27). BSA solution (1.5 g, 8 mL of DI (Deionized water)) added to a solution of triethylenetetraamine (TETA, 0.5 M, 5 mL of DI), pH adjusted to 5 using concentrated HCl and the mixture was stirred for 15 min at room temperature. Then, ethyl-3-(3-(dimethylamino)propyl)carbodiimide (EDC, 1 M, 1 mL in deionized water (DI)) was added, stirred for 4 h and dialyzed against 10 mM sodium phosphate buffer (pH 7.0) using a 25 000 Da cutoff membrane for three times.

Synthesis and Exfoliation of α-ZrP. α-Zr(IV) phosphate was synthesized as reported[37] after appropriate modifications and stacks of the metal phosphate plates were exfoliated with an aqueous solution of tetrabutylammonium hydroxide (TBA) (Supporting Information, Method 1).

Preparation of bZrP. Binding of BSA-TETA(+27) to exfoliated α-ZrP nanosheets was monitored by centrifugation studies by following methods developed in our laboratory (Supporting Information, Method 2)[11] and the data analyzed using the Langmuir adsorption isotherm (eq 1).[15] In eq 1, Γ is the amount of protein adsorbed per surface area of the solid, Γ_m is saturated adsorption, K is the equilibrium constant for the binding process and C is the concentration of proteins.

$$\frac{\Gamma}{\Gamma_m} = \frac{KC}{1 + KC} \quad (1)$$

ζ-Potential Measurements. The ζ-potential titrations were carried out on ZetaPLus (Brookhaven, Holtsville, NY). BSA-TETA(+27) solution (5 μM, 2 μL) was added at a time to a suspension of α-ZrP (6 mM in DI, pH 6, 1.8 mL). The ζ-potential values obtained by the Smoluchowski fit[38] using software supplied by the manufacturer. bZrP was prepared by adding BSA-TETA(+27) into α-ZrP (6 mM) in 10 mM sodium phosphate buffer at pH 7 when the net ζ-potential of the mixture turns to +40 mV and this sample was used for all the subsequent experiments.

Scanning Electron Microscopy (SEM) and Energy-Dispersive X-ray Spectroscopy (EDX) Studies. SEMs were performed using a JEOL JSM-6335F field emission scanning electron microscope and photomicrographs were taken at particular magnifications (Supporting Information, Method 3). EDX was performed on SEM samples using JSM-6335F cold cathode field emission SEM equipped with a Thermo Noran System (JEOL USA Inc., Peabody, MA).

Preparation of Enzyme/bZrP Samples. bZrP samples (10 mM sodium phosphate buffer at pH 7, net charge of +40 mV, Supporting Information, Method 4) contained 30 μM BSA-TETA(+27) and 6 mM α-ZrP were used for enzyme binding, and enzyme binding has been monitored by centrifugation studies, as above.

Powder X-ray Diffraction Studies. Enzyme/bZrP suspensions (in 10 mM sodium phosphate buffer) were drop-casted onto glass slides and air-dried over 2 days (Supporting Information, Method 5). The powder XRD was recorded on a Rigaku Altima IV diffractometer (Woodlands, TX) with Cu Kα radiation (λ = 0.154 06 nm) at the beam voltage and the beam current of 40 kV and 44 mA, respectively. Each sample was scanned at a continuous scan rate of 1°/min and interlayer spacings calculated.

Circular Dichroism (CD) Studies. A Jasco J-710 CD spectrophotometer (Easton, MD) with 0.05 cm path length quartz cuvettes, in the wavelength range of 260−190 nm was used (Supporting Information, Method 6). All spectra were normalized per micro molar bound enzyme per 1 cm path length, and the extent of structure retention has been obtained by comparing these spectra with those of the corresponding unbound proteins, measured under the same conditions.

Enzyme Activity Studies. The catalytic activities of GOX, GOX/α-ZrP and GOX/bZrP were measured using a reported method[7] by monitoring oxidation of D-glucose as the substrate (Supporting Informaiton, Method 7). A pepsin assay[39] was performed with Hb as the substrate. Hb is first denatured by trichloroacetic acid (TCA) and the rate of hydrolysis of denatured Hb by pepsin was measured as a measure of the protease activity of pepsin. Tyrosinase activity[40] of the samples was measured with L-tyrosine as the substrate. Product absorbance at 280 nm was measured for 10 min and the initial absorbancies were used to calculate the initial rates and specific activities. Laccase activity[41] was monitored using syringaldazine as the substrate. The increase in absorbance at 530 nm was measured as a function of time, at room temperature, and initial rates were estimated.

Differential Scanning Calorimetry (DSC). Thermal denaturation of enzyme/bZrP complexes was monitored using a Nano II differential scanning calorimeter (DSC) 6100 (Calorimetry Sciences Corporation CSC, Utah) by following methods developed in our laboratory.[5] DSC traces of enzyme/bZrP samples (10 mM sodium phosphate buffer) with increasing loadings of the enzyme or at constant enzyme loading were recorded. Samples were equilibrated at 20 °C for 10 min and scanned from 20 to 100 °C at a rate of 2 °C/min. The background scan, which was recorded by buffer alone, was subtracted from each sample scan. When denaturation is irreversible, model independent parameters, peak transition temperature (T_m), the temperature where the denaturation begins and $\Delta H_{denaturation}$ (integral $C_p dT$) were extracted from the DSC data.

RESULTS

The α-ZrP nanosheets are attractive nanomaterials for enzyme intercalation, as this improves thermal stabilities and in some cases, activities of biocatalysts.[4] However, α-ZrP has very poor affinity for strongly negatively charged enzymes due to unfavorable electrostatic interactions between the solid and the enzyme. In the current studies, highly cationized BSA-TETA(+27) was preadsorbed on the α-ZrP nanosheets, so that the surface has a net positive charge and provided a variety of amino acid side chains for interactions with acidic enzymes. The cationized-BSA loaded α-ZrP (denoted as bZrP) showed enhanced binding of acidic proteins (Scheme 1) when compared α-ZrP and bound enzyme properties are either improved or retained to a significant extent. These details are presented below.

Cationization of BSA and Binding to α-ZrP. The COOH groups of BSA were modified with triethylenetetra-

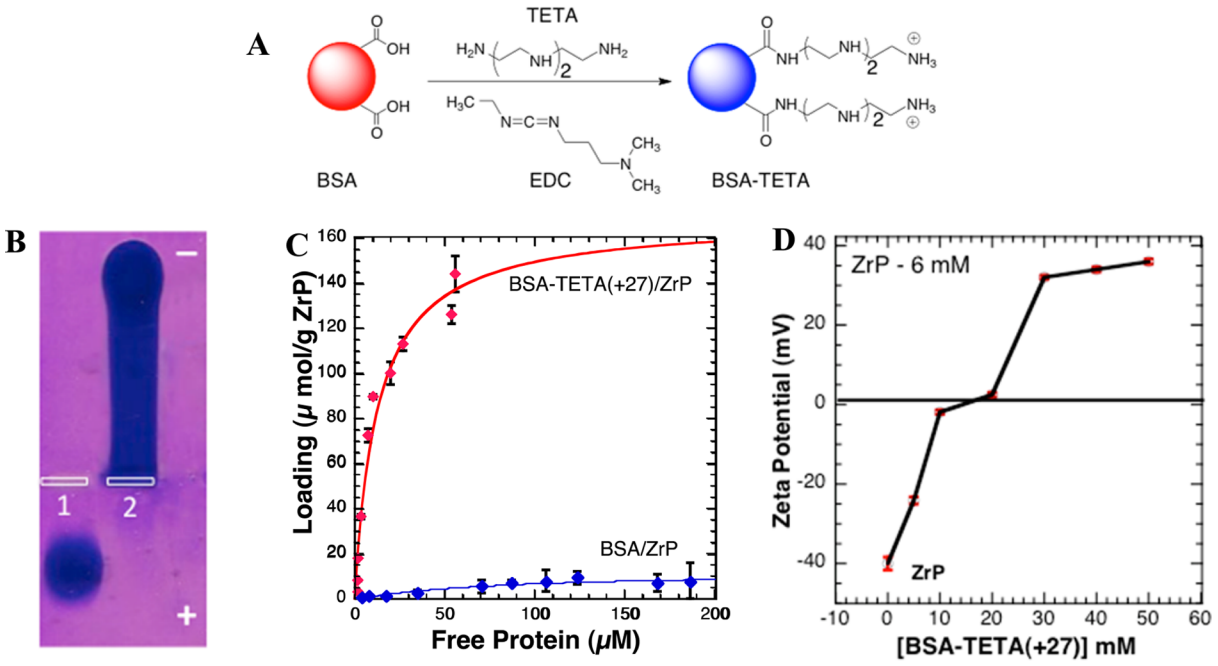

Figure 1. (A) Cationization of BSA by amidation of its carboxylic groups with triethylenetetraamine (TETA) using carbodiimide chemistry. (B) Agarose gel electrophoresis image of BSA (lane 1) and cationized BSA (BSA-TETA(+27) (lane 2). The gel ran at pH 7.0 in 40 mM tris acetate buffer. (C) Binding isotherm of BSA-TETA(+27) (blue dots) and BSA (red dots) binding to α-ZrP. The red line corresponds to best fit to the Langmuir isotherm. (D) The ζ-potential titration of α-ZrP (6 mM) with increasing concentrations of BSA-TETA(+27).

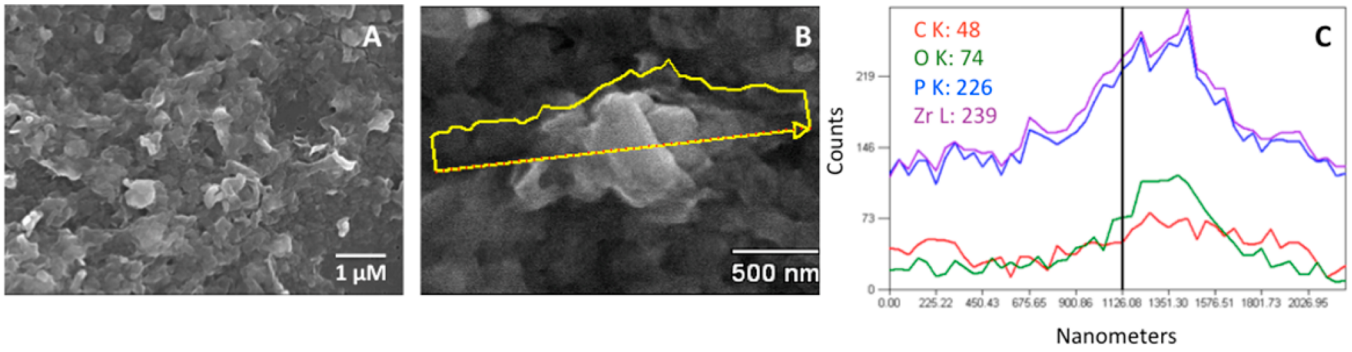

Figure 2. (A) SEM, (B) EDX line image of a single flake of bZrP and (C) elemental microanalysis abundances as a function of distance along the line shown in panel B.

amine (TETA) via carbodiimide chemistry (Figure 1A).[42] The BSA-TETA sample was purified by dialysis to remove unreacted EDC, TETA, and the transformation of negatively charged BSA into a cationic protein was monitored by agarose gel electrophoresis and ζ-potential measurements.

The agarose gel of the pristine BSA (Figure 1B, lane 1) and cBSA purified by dialysis (lane 2) indicated that the negatively charged BSA (pH 7) moved to the positive electrode, whereas the modified BSA moved toward the negative electrode. These data confirm the conversion of the anionic BSA to the corresponding cationized protein. Each TETA side chain can provide multiple positive charges, depending on the pH conditions. The four basic nitrogens present in TETA, for example, can be protonated at particular pH values (pK_{a1} = 3.32, pK_{a2} = 6.67, pK_{a3} = 9.2, pK_{a4} = 9.92) and only three of these will be available for protonation, after conjugation with the COOH group of BSA. Also, note that the pK_a values will be shifted up due to the amidation of one of the TETA nitrogens and hence, each TETA modification could provide only 2−3 positive charges depending on the pH. The electrophoretic mobility of BSA-TETA was taken as the midpoint of the product band, and this mobility was used to calculate the net charge on the product to be +27 relative to that of BSA taken as −18.[2] Due to the finite width of the product band, we estimate a distribution of ±4 units of charge. The charge of BSA-TETA was confirmed by ζ-potential measurements (Supporting Information, Figure 1A) and the sample has been denoted as BSA-TETA(+27) using the charge that corresponded to the midpoint.

The secondary structure of BSA-TETA(+27) was examined by deep UV circular dichroism (CD) spectroscopy and the CD spectrum of the cationized sample matched well with that of the untreated sample (Supporting Information, Figure 1B, red and blue curves, respectively). The BSA-TETA(+27) was then adsorbed on to exfoliated α-ZrP nanosheets and the extent of binding compared with that of BSA (Figure 1C) (red and blue dots, respectively). The binding data were fitted to eq 1, and the association constant (K) as well as saturation binding (B_{max}) obtained. While the binding affinity of BSA to α-ZrP was 7.8 × 10^4 M^{-1}, that of BSA-TETA(+27) increased to 1.2 × 10^5 M^{-1},

dx.doi.org/10.1021/am502070w | ACS Appl. Mater. Interfaces 2014, 6, 9643−9653

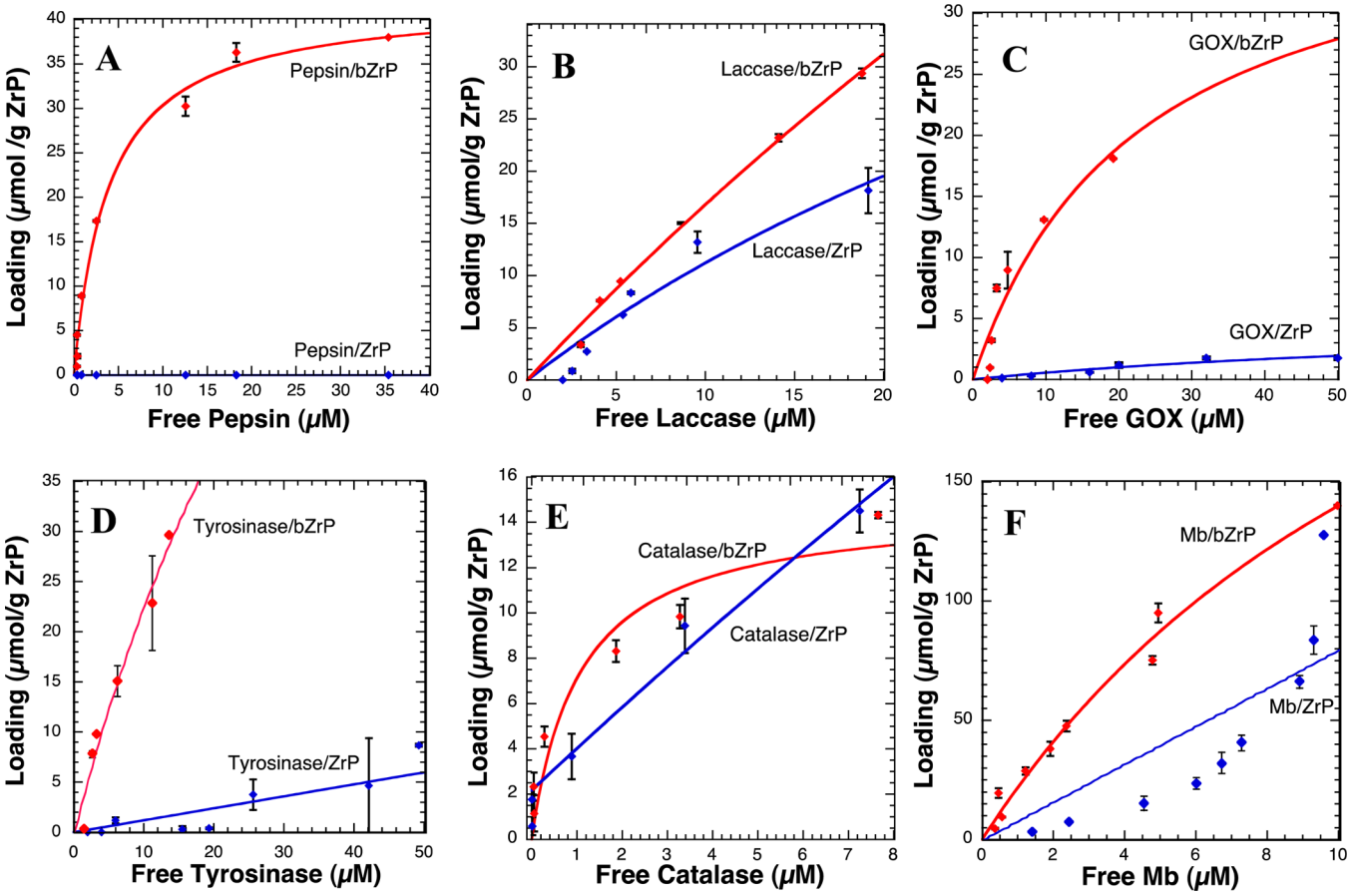

Figure 3. Binding isotherms of (A) pepsin, (B) laccase, (C) GOX, (D) tyrosinase, (E) catalase and (F) Mb with bZrP and α-ZrP (6 mM, error bars are too small in some cases). Langmuir model was used to analyze data and best fits are shown in each case.

and the B_{max} increased from 0.8 ± 0.2 of BSA to 11.2 ± 1.0 g/g for BSA-TETA(+27), a 15-fold improvement for the cationized protein over that of BSA.

The UV CD spectra of bZrP (Supporting Information, Figure 1B) showed that nearly 90% of the cBSA structure was lost upon binding to α-ZrP and hence, protein is unraveled on the nanosheets exposing the amino acid side chains of cBSA for interactions with the solvent or other substances that can be absorbed on bZrP. Binding of cBSA to α-ZrP was also confirmed in ζ-potential measurements. Ionized phosphates on the α-ZrP render it negatively charged (1 charge/25 Å^2) at neutral pH, and the binding of BSA-TETA(+27) is expected to diminish this negative charge or even reverse the net charge. Titration of a suspension of exfoliated α-ZrP nanosheets with aliquots of BSA-TETA(+27) (0−50 μM) indicated a progressive increase in charge from −40 to +38 mV (Figure 1D). Under these conditions, bZrP did not precipitate due to a net positive charge and the suspensions were translucent. We suspected that these surfaces would be more benign for protein binding and facilitate the binding of anionic proteins to the cationic bZrP. The BSA-TETA(+27) adsorbed α-ZrP (bZrP) was further characterized prior to the binding of negatively charged proteins.

Morphology and Elemental Analysis of bZrP. The composition of bZrP was examined by SEM and EDX to gain insight into the location of the protein with respect to the inorganic matrix. SEM micrographs of bZrP at 16000× magnification (Figure 2A) show distinct flakes of zirconium phosphate nanoplates as opposed to the condensed stacks observed for α-ZrP earlier.[5] Further analysis with EDX at 45000× magnification was used to determine the elemental composition profiles, after focusing on a single exfoliated nanoplate. Using the line-count method, which scans across a field of a sample (Figure 2B, arrow), distinct peaks for oxygen and carbon were found at the same region of the plate (Figure 2C). These spikes correlated with the peaks of zirconium and phosphate profiles, which confirmed the presence of the carbon-based protein bound to the α-ZrP nanoplates. The individual bZrP flake displayed in Figure 2B demonstrated the superposition of the elevated zirconium and phosphate elemental signals with those of the carbon and oxygen signals. If the protein was not adsorbed on the inorganic solid, then the carbon signal would have remained significantly lower, as in the surrounding areas.

Enzyme Binding to bZrP: Affinities and Loadings. The above hypothesis of the binding of acidic proteins to cationic bZrP was tested with a small group of anionic proteins with increasing sizes, isoelectric points, surface charge distributions and catalytic activities (Figure 3). Upon binding of pepsin to bZrP, the net charge decreased from +38 to +35 and hence, the overall charge is not neutral. There has been no precipitation of the enzyme/bZrP samples, and they remained as suspensions for several hours. Pepsin is strongly negatively charged (pI = 1) and bound to bZrP even at very low enzyme concentrations (Figure 3A, red dots) while it had essentially no binding to α-ZrP (Figure 3A, blue dots).

A maximum loading of 1.68 g of pepsin per 1 g of bZrP was noted, while there was no binding of pepsin to α-ZrP, under the

dx.doi.org/10.1021/am502070w | ACS Appl. Mater. Interfaces 2014, 6, 9643−9653

same conditions (Figure 3A). These binding data were analyzed with the Langmuir model and the best fit indicated a binding constant of 2.5×10^5 M^{-1}. The maximum loading of pepsin was used to calculate the fraction of the available area occupied by using its area of cross section of 145 Å^2[43] and the surface area of α-ZrP as ~100 m^2/g.[5] The coverage turned out to be about 5.8% of the total available area, and large unoccupied spaces are left out, which could be useful for ingress or egress of reagents/substrates/products.

In a similar fashion, we determined the binding of the remaining enzymes and found that GOX (Figure 3C, red line) and catalase (Figure 3E, red line) bind to bZrP with the affinity constants of 4.4×10^5 and 9.0×10^5 M^{-1}, respectively. GOX binding to bZrP gave a B_{max} of 6.5 g/g, which is much higher than the loading observed for α-ZrP (0.8 g/g). However, catalase and Mb (Figure 3E,F) did not discriminate between bZrP and α-ZrP to a significant extent and the initial sets of data points in these plots indicated significant differences. Strong cooperativity of Mb bindng to α-ZrP is absent with bZrP. Laccase and tyrosinase also showed higher affinities for bZrP when compared to α-ZrP (Figure 2B,C,D,F). Saturation data could not be obtained in many cases, due to the high loadings of protein to bZrP observed here, and protein concentration required to achieve saturation binding far exceeded protein solubilities in the buffer. Therefore, the B_{max} values are only qualitative in these cases and loadings at particular total protein concentrations are used for further analysis.

In addition, we also calculated the highest loadings observed experimentally at the highest total protein concentration used for each protein, with bZrP vs α-ZrP (Figure 4). Pepsin,

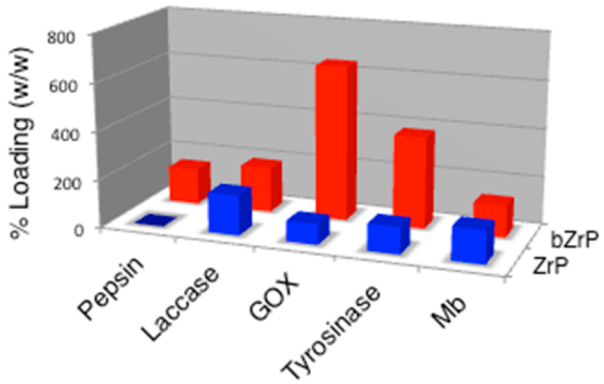

Figure 4. Experimentally observed highest loadings (w/w) of pepsin (100 μM), laccase (64 μM), GOX (100 μM), tyrosinase (64 μM) and Mb (150 μM) to bZrP (6 mM, red bars) and α-ZrP (6 mM, blue bars).

laccase, GOX and tyrosinase showed maximal loadings of 150, 190, 640, 380 and 130 (w/w %) on bZrP, which are higher than the corresponding loadings on α-ZrP except in the case of Mb (0, 170, 85, 110 and 140 w/w %, respectively)

Binding of the anionic proteins to the bZrP could release cBSA into the solution, and this possibility was tested explicitly with GOX. There was no release of cBSA when solutions of GOX (2–20 μM) were equilibrated with bZrP (6 mM with the charge of +38 in 10 mM Na_2HPO_4) as monitored by absorbance of the supernatant at 280 nm, after removing the bound protein from the equilibrated mixture. Therefore, under our binding conditions with GOX, there was no release of cBSA.

Intercalation of Proteins in bZrP. To test the binding of enzymes between the bZrP nanoplates via intercalation, we examined the powder XRD patterns of enzyme/bZrP complexes. If the large enzyme molecules intercalate in the galleries of the bZrP, the gallery spacing should increase by the diameter of the intercalating enzyme. On the other hand, if the binding takes place at the edges of the bZrP, the gallery spacing will be the same as that of bZrP. The interlayer spacings of bZrP (80 Å, Figure 5A, red line) are greater than that of α-ZrP (Figure 5A, inset, 7.6 Å) or that of exfoliated TBA/α-ZrP (Figure 5A, black line, 17 Å).[44] The new peak at the 80 Å is comparable with two of the three dimensions of BSA, 84 × 84 × 35 Å.[45] Upon enzyme binding to bZrP, the spacing was further increased but the peaks were very broad. The extensive broadening of the peaks could be due to the fact that most of these proteins are not perfect spheres and it could also be that the platelets do not stack well. However, the enzyme/bZrP XRD patterns do not show the peaks corresponding to bZrP, TBA/α-ZrP or α-ZrP. Therefore, the absence of the control sample peaks strongly suggests that the enzymes are binding onto the bZrP surface. Binding of pepsin and tyrosinase increased these *d*-spacings to 140 (Figure 5A, blue line) and 117 Å (Figure 5A, green line), respectively. These increases in *d*-spacings are consistent with the intercalation of pepsin and tyrosinase, and data on other systems are not collected.

Bound Enzyme Structure. The extent of retention of the native-like structures of bound enzymes was tested by CD spectroscopy.[46] Using GOX as a model system, we tested the influence of cBSA loading on the extent of structure retention of bound GOX, at a constant concentration of GOX. Thus, several bZrP samples with increasing loadings of of BSA-TETA(+27) (0–35 μM) on α-ZrP (6 mM) with GOX (10 μM) were equilibrated and CD spectra recorded in the deep UV region (Supporting Informaiton, Figure 2B). The secondary structure of GOX gradually improved as a function of increasing BSA-TETA(+27) loading. As estimated from the 22 nm band intensities, the GOX structure improved from 43 to 125% as the BSA-TETA(+27) loading increased from 0 to ~95 (w/w %) of cBSA to α-ZrP. Under these conditions, the CD spectrum of GOX/bZrP showed its characteristic minima at 210 and 222 nm (Figure 5B, light blue line), which more or less, overlapped with that of GOX (Figure 5B, dark blue line). In control experiments, cBSA bound to α-ZrP had no detectable CD, under similar conditions. Hence, bZrP samples with 90% w/w loading of BSA-TETA(+27) to α-ZrP were used for all subsequent studies. For example, the extents of structure retention of pepsin, laccase and tyrosinase bound to bZrP were nearly 98–100% (Figure 5C).

Activities. The effect of biofunctionalization of α-ZrP on the catalytic activities of the bound enzymes was compared with those of the enzymes bound to α-ZrP (Figure 6). Product formation for each of these catalytic reactions were monitored by appropriate methods and the specific rates calculated and compared. For example, the kinetic traces for the GOX, GOX/ZrP and GOX/bZrP are compared in Figure 6A, which are nearly the same. The initial rates of these reactions, as obtained from the slope of the tangent to the curve at zero reaction time, are then used to calculate the corresponding specific activities (Figure 6B). All activities of the enzyme/bZrP complexes are nearly comparable to those of the corresponding free enzymes and enzyme/α-ZrP samples, with the exception of tyrosinase.

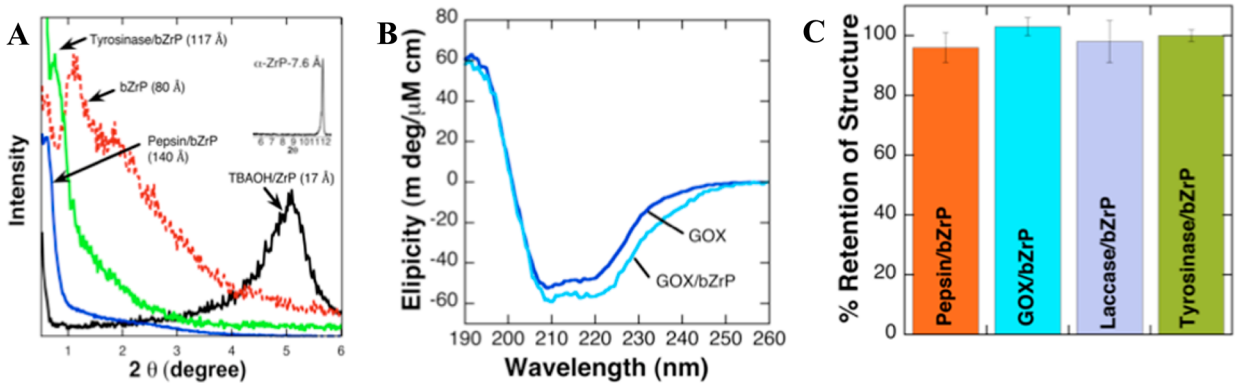

Figure 5. (A) Powder XRD patterns of α-ZrP (inset), exfoliated α-ZrP (TBA/α-ZrP) (black line), bZrP (red line), pepsin/bZrP (blue line) and tyrosinase/bZrP (green line). Corresponding d-spacings are shown in parentheses on each curve. (B) The far UV CD spectra of GOX (dark blue line) and GOX/bZrP (light blue line). (C) The % retention of secondary structure of protein/bZrP samples measured by comparing ellipticity at 222 nm with that of the unbound protein.

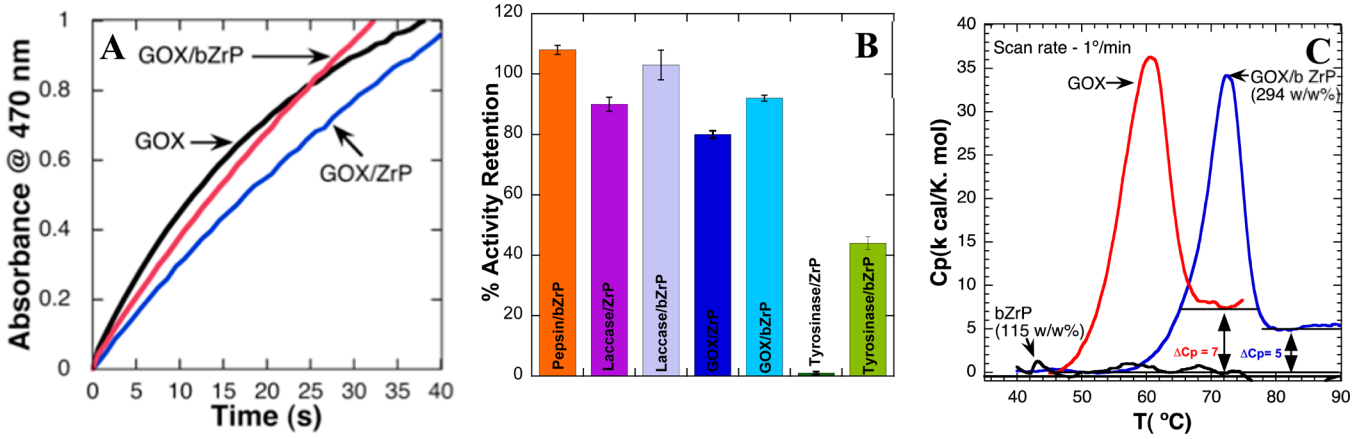

Figure 6. (A) Activities of GOX/bZrP (red line), GOX/α-ZrP (blue line) and GOX (black line) measured by kinetic traces monitoring the absorbance at 470 nm. (B) The retention of the enzymatic activities of enzyme/bZrP and enzyme/α-ZrP complexes in comparison to their respective free enzymes. (C) DSC thermograms of GOX (red), GOX/bZrP (blue) and bZrP (black). The BSA-TETA(+27) and GOX loading are shown in parentheses.

Binding of tyrosinase to α-ZrP essentially deactivated the enzyme while bZrP restored the activity to a significant extent (>40%). Thus, biofunctionalization of α-ZrP had a significant effect on tyrosinase activity.

Thermal Stabilities of Enzyme/bZrP Complexes. Another important attribute for biocatalysts is their thermal stability and passivation of high-energy sites on the solid with cBSA is expected to enhance the bound enzyme stabilities. DSC provides quantitative measurements of the denaturation enthalpy (ΔH) and the denaturation temperature (T_m), in a model independent manner. The DSC profiles of GOX and GOX/bZrP are compared in Figure 6C.

Thermogram of GOX/bZrP (Figure 6C, blue line, ~300 g/g) shows that the enzyme begins to denature at 60 °C with a maximum at 72 °C and continues to denature up to 80 °C with a relatively sharp thermal transition. On the other hand, GOX started to denature at 45 °C and continued up to 66 °C (Figure 6C, red line). Any contribution of bZrP to these profiles is negligible (Figure 6C, black line) as cBSA loaded on the solid is completely denatured (see Circular Dichroism (CD) Studies). The areas under the curves (ΔH) for GOX and GOX/bZrP gave the corresponding denaturation enthalpies to be 319 and 250 kcal/mol, respectively.

DSC profiles of GOX/bZrP were examined as a function of GOX loading (~90 to ~300 w/w %), and the T_m gradually increased from 60 to 72 °C (Supporting Information, Figure 4), while thermal transitions became progressively sharper with concomitant increases in ΔH. Thus, GOX retained better structure and higher thermal stabilities, as its loading was increased.

In contrast to GOX, intercalation of pepsin in bZrP (80 w/w %), however, lead to lower thermal stability. Both T_m and ΔH decreased (58 to 48 °C and 92 to 60 kcal/mol, respectively, Supporting Information, Figure 5A). The DSC profiles of laccase and tyrosinase (pH 7.0, 1 mg/mL) had multiple transitions, which were previously assigned to multiple domains.[47] Tyrosinase/bZrP (50 w/w %) indicated a small increase in T_m from 72 to 76 °C (Supporting Information, Figure 5CB). Laccase had a major denaturation transition at 85 °C with ΔH of ~20 kcal/mol and laccase/bZrP (125 w/w %) indicated no change in T_m but ΔH increased 9-fold (Supporting Information, Figure 5C). On the whole, GOX, tyrosinase and laccase indicated improved thermal stabilities while pepsin was marginally destabilized by bZrP.

Overall, coating of α-ZrP nanosheets by simple, one-step preadsorption of cBSA expanded the use of α-ZrP for enhanced

protein loading while maintaining their native-like structures and activities with enhanced thermal stabilities in specific cases.

DISCUSSION

Previous investigations positioned α-ZrP as an effective solid platform for protein and enzyme binding with improved thermal stabilities and even enhanced activities when compared to the corresponding unbound enzymes.[1,24] One advantage of this solid was its strong negative charge field, which binds a number of positively charged proteins as well as marginally negatively charged proteins. However, strongly negatively charged enzymes such as the ones examined here, except laccase and catalase, bind poorly to α-ZrP due to unfavorable electrostatic interactions. Preadsorption of α-ZrP with a sacrificial, strongly cationized BSA overcomes this electrostatic barrier and also provides a variety of amino acid side chains for favorable interactions with the binding enzyme.

BSA is often used to suppress nonspecific binding of proteins to solid surfaces, but the chemical modification of BSA with the polyamine and its adsorption on α-ZrP increased the affinities of a variety of proteins, where the cationized BSA functioned as the protein glue. bZrP, for example, indicated enhanced binding of pepsin, GOX, tyrosinase and Mb, whereas laccase and catalase had comparable affinities with both solids. This improvement in the binding of anionic proteins to bZrP is a result of the charge reversal where cBSA acted as an excellent anchor where it bound to both the anionic α-ZrP surface as well as the anionic enzymes. This approach appears to be universal for binding anionic proteins, as all the samples examined here with a wide range of pI values and molecular weights and shapes indicated good binding to bZrP.

Powder XRD data (Figure 5A, red line) indicated an average thickness of the BSA-TETA(+27) layer on α-ZrP at 350% (w/w) to be 80 Å, and this layer is thicker than the average diameter of BSA (62 Å).[48] At the highest loading cBSA of 500% (w/w) observed (Figure 1C), there could be multiple layers of BSA that are stretched out. The binding of BSA-TETA(+27) to α-ZrP was confirmed by ζ-potential titrations where the charge changes from −40 to +38 mV (Figure 1C). After the charge on the α-ZrP surface was fully neutralized, protein binding continued. This process resulted in an accumulation of excess positive charge on the bZrP nanosheets. A similar phenomenon, overcharging of the surface, was observed during polyion binding to DNA, which may be considered as a one-dimensional analogue of α-ZrP, and also in the layer-by-layer assembly of polymer polyelectrolytes.[49] The bZrP served as a cationic analogue for the binding of anionic enzymes where the loading capacity has been substantially improved.

In contrast to the preferential binding of pepsin, GOX and tyrosinase to bZrP, laccase and catalase showed comparable loadings to both solids. One possible reason might be that the positively charged patches on these enzymes (Scheme 1) facilitate binding to the anionic α-ZrP while the negatively charged patches favor binding to bZrP. However, their isotherms display a linear increase in loading with the initial enzyme concentration without saturation, even at very high protein concentrations.

The above enzyme loadings, in general, far exceeded those known for other solid supports. For instance, pepsin binding to alumina nanoparticles (20 nm) gave a maximum loading of 0.13 g/1g of pepsin to alumina,[50] which is far less than the 150% w/w loading observed here. Among various carbon-based materials used for GOX loading, mesocellular carbon form showed only 40% (w/w GOX to carbon) maximum loading[51] when compared to the 640% w/w observed in the current studies with bZrP. A recent study also shows that the covalent immobilization of tyrosinase on carbon nanopowder and single-walled carbon nanotubes with maximum loadings of only 210% w/w,[52] which is below the 380% w/w loading observed here, with bZrP.

Powder XRD studies indicated that the binding of proteins to bZrP could be via the intercalation mode, which we have previously shown to be the case for protein binding to α-ZrP. Observed *d*-spacing for protein/α-ZrP complexes was attributed to the intercalation of a monolayer of the protein and several layers of water molecules.[32] The *d*-spacing observed for pepsin/bZrP (140 Å) in the current studies is much higher than the *d*-spacing of bZrP (80 Å) plus the reported dimensions of the pepsin (70 × 40 × 30 Å).[54] Also, note that the pepsin loading saturated around 150% w/w and therefore, these observations taken together suggest that the on coming protein resides on the preadsorb underlying cBSA layer. The broad peaks suggest the platelets do not assemble in a well-ordered manner but *d*-spacings corresponding to bZrP or α-ZrP are not noted here. Therefore, protein binding on the bZrP nanosheets is strongly suggested. The *d*-spacing noted for tyrosinase/bZrP (117 Å) also supports the idea that these proteins bind on top of cBSA layer, and in the case of GOX/bZrP the spacings were too large to be measured.

The UV CD data showed that all four enzyme/bZrP samples examined here retained most of their native-like structures (Figure 5C, Supporting Information, Figure 2A). Structure distortion is often observed on binding of most proteins to most of the solid surfaces. For example, GOX underwent extensive conformational changes with decreasing α-helicity and excessive unfolding upon binding to graphene oxide.[53] In contrast, some conformational changes of protein were noticed when hemoglobin or myoglobin bind to bare α-ZrP and cointercalation of these proteins with DNA improved their structure retention considerably.[6] Hence, the underlying BSA-TETA(+27) layer in bZrP provided a benign environment for the bound proteins by blocking high energy sites on solid surfaces. If not blocked, these sites may contribute to the protein denaturation and this conclusion was also supported by the extensive retention of bZrP-bound enzyme activities.

The specific activity of pepsin bound to bZrP is comparable to that of unbound pepsin (3.0×10^{-2} μM^{-1} vs 2.8×10^{-2} μM^{-1}, Supporting Information, Table 2). Catalytic activity of pepsin/bZrP requires that the substrate (Hb) bind to the active site cleft in the bilobal structure of pepsin. Hence, the gallery spacing of 140 Å noted in the XRD studies for this biocatalyst is large enough for the ingress−egress of the large substrate. Among various solid supports used for immobilizing pepsin, a recent study shows only 22% retention of pepsin activity on SBA-15 mesoporous silica while using the same substrate used here, Hb.[54] Hence, in comparison to other solids, pepsin retained higher activity on bZrP nanolayers.

Complete retention of activity was also observed for the laccase/bZrP complex (2.2×10^{-2} μM^{-1} vs 2.1×10^{-2} μM^{-1}), which is much higher when compared to reported activity retention of 26−64% observed for laccase adsorbed on inorganic minerals.[55] The specific activities of GOX, GOX/α-ZrP and GOX/bZrP (3×10^{-2}, 2.8×10^{-2} and 2.5×10^{-2} μM^{-1}, respectively) are essentially the same as the unbound enzyme, whereas only 25% of specific activity was retained when immobilized onto multiwall carbon nanotubes, which

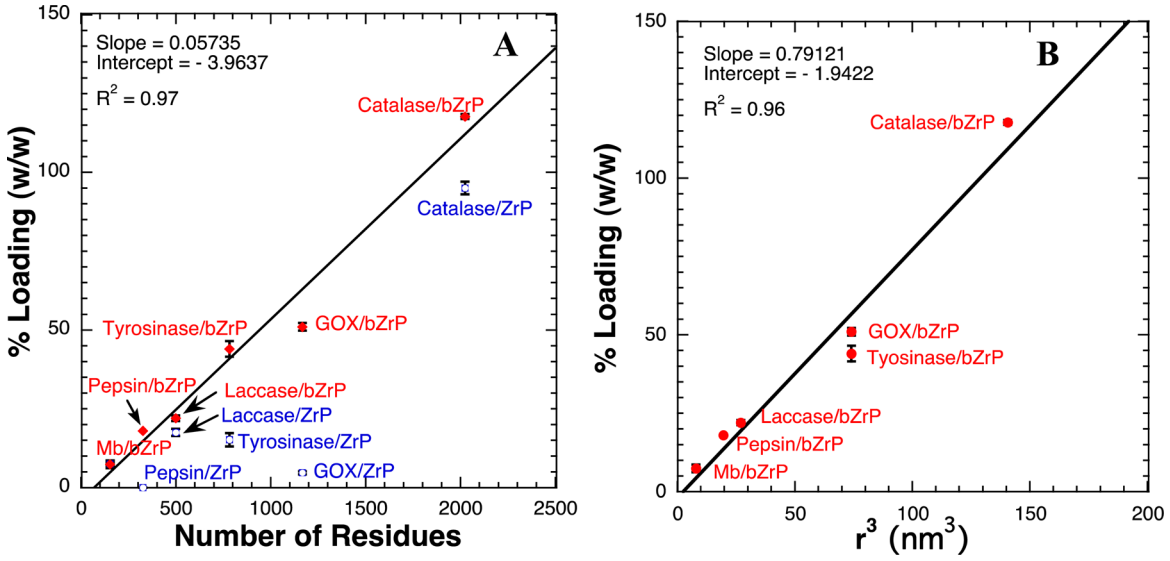

Figure 7. Plot of enzyme loading on bZrP vs (A) number of residues and (B) volume of the enzyme. In each case, 6 mM bZrP or α-ZrP was used, and all loadings were calculated at 8 μM of total protein concentration to avoid any protein−protein interactions or cooperativity effects.

improved to 65% upon covalent immobilization using a PEG linker.[56] Although complete activity loss was noted for tyrosinase/α-ZrP, tyrosinase/bZrP retained 50% of its activity and tyrosinase entrapped on molecular sieves, silica gel, alumina-G, sepharose beads showed <40% retention of activity.[57] However, it is known that tyrosine oxidation by this enzyme exhibits an initial lag phase, which is known to be shortened or even eliminated by the addition of catalytic amounts of *o*-diphenol or transition metal ions.[58] This initial lag phase is absent for tyrosinase/bZrP, which is a considerable additional advantage of the current approach (Supporting Information, Figure 3A).

The benign nature of the bZrP interactions with the bound enzymes was further confirmed by the DSC data (Supporting Information, Table 3). Constraining enzymes within the two-dimensional space of α-ZrP improved thermal stabilities of the intercalated proteins.[59] However, these thermograms showed extensive broadening, which was attributed to the heterogeneity in the bound enzyme population, and hence, the situation is expected to improve by blocking the high-energy sites with cBSA, providing a more benign environment rather than the phosphate lattice of the bare α-ZrP. The DSC studies of GOX/bZrP and other proteins confirmed the positive effect of surrounding protein-o-philic environment of bZrP on the improved thermal stability, which is accompanied by the sharper denaturation transitions in multiple cases. These observations are in contrast to the extensive broad DSC profiles reported for protein/α-ZrP samples, in our previous studies.[5]

The binding interaction is more complex than expected from a simple electrostatic model, where the binding or the loading should scale with increase in the negative charge of the enzyme, as bZrP is strongly positively charged. The binding affinities or the loadings with bZrP had no correlation with the pI or the net charge of the protein or the charge of the complex formed (Supporting Information, Figure 6). However, the loading on bZrP showed a strong linear correlation with the number of residues present on the enzyme (Figure 7A, red dots, R = 0.97) where the number of residues increased from ∼153 to 2024 with the current set of proteins. A comparison of the corresponding loadings to α-ZrP (blue dots) indicated considerable scatter. A linear fit to the bZrP data (red line) indicated a slope of 0.06% loading per residue and nonzero intercept, and loading also increased linearly with number of residues at higher protein loadings (Supporting Information, Figure 7). These data suggest that the loading increases linearly with the number of residues or that the binding interaction with bZrP is intrinsic to the interactions with the amino acid side chains of the incoming enzyme, rather than other properties. This conclusion and the goodness of the fit with R = 0.97 is significant, as this provides a powerful new tool to predict loadings of a given enzyme for bZrP simply based on the number of residues present. To the best of our knowledge, this is the first report of residue-dependent protein loading at a given nano-bio interface.

To test if the above correlation is due to gradual increase in the size of the enzyme with increasing number of residues, we investigated the correlation between the loading and the size of the enzyme (Figure 7B). As the size increases, the number of possible contacts that can be made between the enzyme and the solid surface also increases we observed a strong linear correlation (R = 0.96) having a slope of 0.8% w/w loading per unit volume of the enzyme. Because the volume of a sphere is proportional to its area of cross-section, the contact area between a spherical protein and planar bZrP nanosheets should increase linearly with the number of residues. This increase in the contact area should also increase in the number of interactions between the protein and the nanosheet and thereby increase the affinity or the loading of the protein on bZrP. Hence, the volume of the enzyme, which increases with increasing the number of residues,[60] can be used as a measure of its loading capacity on the bZrP surface but note the differences in the intercepts. One minor difference between the two plots is the small difference in the *y*-intercepts. However, these are too small to discuss and well within our experimental errors.

In contrast to pristine α-ZrP, which has shown low affinity for negatively charged biomolecules, cationic bZrP improved the binding of negatively charged enzymes with an exceptional loading capacity while retaining nearly 100% structure and

activity. Thus, the current method of coating the nanosheets with cBSA to alter its net charge as well as the surface characteristics provides a good foundation to improve the functionalities of nanomaterials as benign supports for enzyme binding in a predictable manner.

CONCLUSIONS

Current results illustrate the biofunctionalization of α-ZrP with a protein glue and its effect on enzyme/protein binding on the modified surface compared to that of pristine surface. Conversion of a homogeneous inorganic nanosurface inherently decorated with phosphate groups into a pool of amino acid side chains enhanced the effectiveness for enzyme binding. As a result, many acidic enzymes showed greater affinities toward bZrP while maintaining native-like structures and activities.

On the other hand, binding to biofuntionalized or even the pristine surface did not show a direct correlation with the net charge of the enzyme, which suggests that the electrostatic interactions are not dominant factors. The enzyme loadings on bZrP revealed a strong connection to the number of residues and protein sizes, but these two parameters are inter-related. Nevertheless, the conclusion is that the current approach provides a predictable quantitative method for enzyme loading on these surfaces, for the first time, at least for anionic proteins, given some caveats. A fundamental insight is gained in these systems, and biofunctioanlization, as developed here, provides added value to the natural surface and these insights are important to regulate the nano-bio interfaces to construct biofunctional materials while ensuring their biological structure and activity retention.

ASSOCIATED CONTENT

Supporting Information

Extinction coefficients used to calculate the concentration of unbound enzyme in the supernatants, ζ-potential of BSA-TETA, CD plots, kinetic plots, binding curves and DSC thermograms. This material is available free of charge via the Internet at http://pubs.acs.org.

AUTHOR INFORMATION

Corresponding Author

*C. V. Kumar. E-mail: Challa.Kumar@Uconn.edu.

Notes

The authors declare no competing financial interest.

ACKNOWLEDGMENTS

C.V.K. thanks NSF (DMR-BMAT-1005609) for financial support.

REFERENCES

(1) Liu, X.; Chen, X.; Li, Y.; Wang, X.; Peng, X.; Zhu, W. Preparation of Superparamagnetic Fe_3O_4@Alginate/Chitosan Nanospheres for Candida Rugosa Lipase Immobilization and Utilization of Layer-by-Layer Assembly to Enhance the Stability of Immobilized Lipase. *ACS Appl. Mater. Interfaces* **2012**, *4*, 5169−5178.

(2) Bellino, M. G.; Regazzoni, A. E.; Soler-Illia, G. J. A. A. Amylase-Functionalized Mesoporous Silica Thin Films as Robust Biocatalyst Platforms. *ACS Appl. Mater. Interfaces* **2010**, *2*, 360−365.

(3) Sun, X.; Zhao, Y.; Lin, V. S. Y.; Slowing, I. I.; Trewyn, B. G. Luciferase and Luciferin Co-immobilized Mesoporous Silica Nanoparticle Materials for Intracellular Biocatalysis. *J. Am. Chem. Soc.* **2011**, *133*, 18554−18557.

(4) Jin, L.; Yang, K.; Yao, K.; Zhang, S.; Tao, H.; Lee, S.-T.; Liu, Z.; Peng, R. Funtionalized Graphene Oxide in Enzyme Engineering: A Selective Modulator for Enzyme Activity and Thermostability. *ACS Nano* **2012**, *6*, 4864−4875.

(5) Deshapriya, I. K.; Kumar, C. V. Nanobio Interfaces: Charge Control of Enzyme/Inorganic Interfaces for Advanced Biocatalysis. *Langmuir* **2013**, *29*, 14001−14016.

(6) Mudhivarthi, V. K.; Bhambhani, A.; Kumar, C. V. Novel Enzyme/DNA/Inorganic Nanomaterials: a New Generation of Biocatalysts. *Dalton Trans.* **2007**, 5483−5497.

(7) Bellezza, F.; Cipiciani, A.; Costantino, U. Esterase Activity of Biocomposites Constituted by Lipases Adsorbed on Layered Zirconium Phosphate and Phosphonates: Selective Adsorption of Different Enzyme Isoforms. *J. Mol. Catal. B: Enzym.* **2003**, *26*, 47−56.

(8) Pattammattel, A.; Deshapriya, I. K.; Chowdhury, R.; Kumar, C. V. Metal-Enzyme Frameworks: Role of Metal Ions in Promoting Enzyme Self-Assembly on α-Zirconium(IV) Phosphate Nanoplates. *Langmuir* **2013**, *29*, 2971−2981.

(9) Hartwig, A. Zinc Finger Proteins As Potential Targets for Toxic Metal Ions: Differential Effects On Structure and Function. *Antioxid. Redox Signaling* **2001**, *3*, 625−34.

(10) Malgieri, G.; Grasso, G. The Clearance of Misfolded Proteins in Neurodegenerative Diseases by Zinc Metalloproteases: An Inorganic Perspective. *Coord. Chem. Rev.* **2014**, *260*, 139−155.

(11) Chowdhury, R.; Stromer, B.; Pokharel, B.; Kumar, C. V. Control of Enzyme−Solid Interactions via Chemical Modification. *Langmuir* **2012**, *28*, 11881−11889.

(12) Koblinski, J. E.; Wu, M.; Demeler, B.; Jacob, K.; Kleinman, H. K. Matrix Cell Adhesion Activation by Non-Adhesion Proteins. *J. Cell Sci.* **2005**, *118*, 2965−74.

(13) Khan, W.; Kapoor, M.; Kumar, N. Covalent Attachment of Proteins to Functionalized Polypyrrole-Coated Metallic Surfaces for Improved Biocompatibility. *Acta Biomater.* **2007**, *3*, 541−549.

(14) Liu, J.; Fu, S.; Yuan, B.; Li, Y.; Deng, Z. Toward a Universal "Adhesive Nanosheet" for the Assembly of Multiple Nanoparticles Based on a Protein-Induced Reduction/Decoration of Graphene Oxide. *J. Am. Chem. Soc.* **2010**, *132*, 7279−7281.

(15) Wassell, D. T. H.; Hall, R. C.; Embery, G. Adsorption of Bovine Serum Albumin on to Hydroxyapatite. *Biomaterials* **1995**, *16*, 697−702.

(16) Wassell, D. T. H.; Embery, G. Adsorption of Bovine Serum Albumin on to Titanium Powder. *Biomaterials* **1996**, *17*, 859−864.

(17) Larsericsdotter, H.; Oscarsson, S.; Buijs, J. Structure, Stability, and Orientation of BSA Adsorbed to Silica. *J. Colloid Interface Sci.* **2005**, *289*, 26−35.

(18) Wang, Y.; Li, Z.; Wang, J.; Li, J.; Lin, Y. Graphene and Graphene Oxide: Biofunctionalization and Applications in Biotechnology. *Trends Biotechnol.* **2011**, *29*, 205−212.

(19) Brewer, S. H.; Glomm, W. R.; Johnson, M. C.; Knag, M. K.; Franzen, S. Probing BSA Binding to Citrate-Coated Gold Nanoparticles and Surfaces. *Langmuir* **2005**, *21*, 9303−9307.

(20) Kumar, C. V.; Duff, M. R. DNA-Based Supramolecular Artificial Light Harvesting Complexes. *J. Am. Chem. Soc.* **2009**, *131*, 16024−16026.

(21) Kumar, C. V.; Duff, J. M. R. Towards Building Artificial Light Harvesting Complexes: Enhanced Singlet-Singlet Energy Transfer Between Donor and Acceptor Pairs Bound to Albumins. *Photochem. Photobiol. Sci.* **2008**, *7*, 1522−1530.

(22) Kondo, A.; Oku, S.; Higashitani, K. Structural Changes in Protein Molecules Adsorbed on Ultrafine Silica Particles. *J. Colloid Interface Sci.* **1991**, *143*, 214−221.

(23) McClellan, S. J.; Franses, E. I. Adsorption of Bovine Serum Albumin at Solid/Aqueous Interfaces. *Colloids Surf., A* **2005**, *260*, 265−275.

(24) Larsericsdotter, H.; Oscarsson, S.; Buijs, J. Structure, Stability, and Orientation of BSA Adsorbed to Silica. *J. Colloid Interface Sci.* **2005**, *289*, 26−35.

(25) Pattammattel, A.; Puglia, M.; Chakraborty, S.; Deshapriya, I. K.; Dutta, P. K.; Kumar, C. V. Tuning the Activities and Structures of

Enzymes Bound to Graphene Oxide with a Protein-glue. *Langmuir* **2013**, *29*, 2971−2981.
(26) Bovey, F.; Yanari, S. *Pepsin, The Enzymes*, 2nd ed.; Academic Press, Inc., New York, 1960.
(27) Hublik, G.; Schinner, F. Characterization and Immobilization of the Laccase from *Pleurotus ostreatus* and its Use for the Continuous Elimination of Phenolic Pollutants. *Enzyme Microb. Technol.* **2000**, *27*, 330−336.
(28) Pazur, J. H.; Kleppe, K. The Oxidation of Glucose and Related Compounds by Glucose Oxidase from Aspergillus niger. *Biochemistry* **1964**, *3*, 578−583.
(29) Zhu, Y.; Kaskel, S.; Shi, J.; Wage, T.; van Pée, K.-H. Immobilization of Trametes versicolor Laccase on Magnetically Separable Mesoporous Silica Spheres. *Chem. Mater.* **2007**, *19*, 6408−6413.
(30) Min, D.; Zhang, X.; He, W.; Zhang, Y.; Li, P.; Zhang, M.; Liu, J.; Liu, S.; Xu, F.; Du, Y.; Zhang, Z. Direct Immobilization of Glucose Oxidase in Magnetic Mesoporous Bioactive Glasses. *J. Mater. Chem. B* **2013**, *1*, 3295−3303.
(31) Wang, J. Electrochemical Glucose Biosensors. *Chem. Rev.* **2007**, *108*, 814−825.
(32) Kumar, C. V.; Chaudhari, A. Proteins Immobilized at the Galleries of Layered α-Zirconium Phosphate: Structure and Activity Studies. *J. Am. Chem. Soc.* **2000**, *122*, 830−837.
(33) Zhu, Y.; Kaskel, S.; Shi, J.; Wage, T.; van Pée, K.-H. Immobilization of Trametes versicolor Laccase on Magnetically Separable Mesoporous Silica Spheres. *Chem. Mater.* **2007**, *19*, 6408−6413.
(34) Atalla, M. M.; Zeinab, H. K.; Eman, R. H.; Amani, A. Y.; Abeer, A. A. E. A. Characterization and Kinetic Properties of the Purified Trematosphaeria Mangrovei Laccase Enzyme. *Saudi J. Biol. Sci.* **2013**, *20*, 373−381.
(35) Palumbo, A.; Misuraca, G.; D'Ischia, M.; Prota, G. Effect of Metal Ions on the Kinetics of Tyrosine Oxidation Catalysed by Tyrosinase. *Biochem. J.* **1985**, *228*, 647−651.
(36) Lobo, V.; Patil, A.; Phatak, A.; Chandra, N. Free Radicals, Antioxidants and Functional Foods: Impact on Human Health. *Pharmacogn Rev.* **2010**, *4*, 118−26.
(37) Clearfield, A.; Stynes, J. A. The Preparation of Crystalline Zirconium Phosphate and Some Observations on its Ion Exchange Behavior. *J. Inorg. Nucl. Chem.* **1964**, *26*, 117−129.
(38) Sze, A.; Erickson, D.; Ren, L.; Li, D. Zeta-Potential Measurement Using the Smoluchowski Equation and the Slope of the Current-Time Relationship in Electroosmotic Flow. *J. Colloid Interface Sci.* **2003**, *261*, 402−10.
(39) Anson, M. The Estimation of Pepsin, Trypsin, Papain and Cathepsin with Hemoglobin. *J. Gen. Physiol.* **1938**, *22*, 79−89.
(40) Duckworth, H. W.; Coleman, J. E. Physicochemical and Kinetic Properties of Mushroom Tyrosinase. *J. Biol. Chem.* **1970**, *245*, 1613−1625.
(41) Ride, J. P. The effect of Induced Lignification on the Resistance of Wheat Cell Walls to Fungal Degradation. *Physiol. Plant Pathol.* **1980**, *16*, 187−196.
(42) Thilakarathne, V. K.; Briand, V. A.; Kasi, R. M.; Kumar, C. V. Tuning Hemoglobin−Poly(acrylic acid) Interactions by Controlled Chemical Modification with Triethylenetetramine. *J. Phys. Chem. B* **2012**, *116*, 12783−12792.
(43) Min, K.; Kim, J.; Park, K.; Yoo, Y. J. Enzyme Immobilization on Carbon Nanomaterials: Loading Density Investigation and Zeta Potential Analysis. *J. Mol. Catal. B: Enzym.* **2012**, *83*, 87−93.
(44) Clearfield, A.; Duax, W. L.; Medina, A. S.; Smith, G. D.; Thomas, J. R. Mechanism of Ion Exchange in Crystalline Zirconium Phosphates. I. Sodium Ion Exchange of Alpha-Zirconium Phosphate. *J. Phys. Chem.* **1969**, *73*, 3424−3430.
(45) Li, N.; Zeng, S.; He, L.; Zhong, W. Probing Nanoparticle−Protein Interaction by Capillary Electrophoresis. *Anal. Chem.* **2010**, *82*, 7460−7466.
(46) Saxena, V. P.; Wetlaufer, D. B. A New Basis for Interpreting the Circular Dichroic Spectra of Proteins. *Proc. Natl. Acad. Sci. U. S. A.* **1971**, *68*, 969−972.
(47) Toledo-Núñez, C.; López-Cruz, J. I.; Hernández-Arana, A. Thermal Denaturation of a Blue-Copper Laccase: Formation of a Compact Denatured State with Residual Structure Linked to pH Changes in the Region of Histidine Protonation. *Biophys. Chem.* **2012**, *167*, 36−42.
(48) González Flecha, F. L.; Levi, V. Determination of the Molecular Size of BSA by Fluorescence Anisotropy. *Biochem Mol. Biol. Educ.* **2003**, *31*, 319−322.
(49) Rawat, K.; Pathak, J.; Bohidar, H. B. Effect of Persistence Length on Binding of DNA to Polyions and Overcharging of Their Intermolecular Complexes in Aqueous and in 1-methyl-3-octyl Imidazolium Chloride Ionic Liquid Solutions. *Phys. Chem. Chem. Phys.* **2013**, *15*, 12262−12273.
(50) Li, J.; Wang, J.; Gavalas, V. G.; Atwood, D. A.; Bachas, L. G. Alumina−Pepsin Hybrid Nanoparticles with Orientation-Specific Enzyme Coupling. *Nano Lett.* **2002**, *3*, 55−58.
(51) Lee, D.; Lee, J.; Kim, J.; Kim, J.; Na, H. B.; Kim, B.; Shin, C. H.; Kwak, J. H.; Dohnalkova, A.; Grate, J. W.; Hyeon, T.; Kim, H. S. Simple Fabrication of a Highly Sensitive and Fast Glucose Biosensor Using Enzymes Immobilized in Mesocellular Carbon Foam. *Adv. Mater.* **2005**, *17*, 2828−2833.
(52) Min, K.; Kim, J.; Park, K.; Yoo, Y. J. Enzyme Immobilization on Carbon Nanomaterials: Loading Density Investigation and Zeta Potential Analysis. *J. Mol. Catal. B: Enzym.* **2012**, *83*, 87−93.
(53) Shao, Q.; Wu, P.; Xu, X.; Zhang, H.; Cai, C. Insight into the Effects of Graphene Oxide Sheets on the Conformation and Activity of Glucose Oxidase: Towards Developing a Nanomaterial-Based Protein Conformation Assay. *Phys. Chem. Chem. Phys.* **2012**, *14*, 9076−9085.
(54) Manyar, H. G.; Gianotti, E.; Sakamoto, Y.; Terasaki, O.; Coluccia, S.; Tumbiolo, S. Active Biocatalysts Based on Pepsin Immobilized in Mesoporous SBA-15. *J. Phys. Chem. C* **2008**, *112*, 1810−18116.
(55) Wu, Y.; Jiang, Y.; Jiao, J.; Liu, M.; Hu, F.; Griffiths, B. S.; Li, H. Adsorption of Trametes versicolor laccase to Soil Iron and Aluminum Minerals: Enzyme Activity, Kinetics and Stability Studies. *Colloids Surf., B* **2014**, *114*, 342−348.
(56) Campbell, A. S.; Dong, C.; Meng, F.; Hardinger, J.; Perhinschi, G.; Wu, N.; Dinu, C. Z. Enzyme Catalytic Efficiency is a Function of Bio-Nano Interface Reactions. *ACS Appl. Mater. Interfaces* **2014**, *6*, 5393−5403.
(57) Durán, N.; Rosa, M. A.; D'Annibale, A.; Gianfreda, L. Applications of Laccases and Tyrosinases (Phenoloxidases) Immobilized on Different Supports: a Review. *Enzyme Microb. Technol.* **2002**, *31*, 907−931.
(58) Chang, T.-S. An Updated Review of Tyrosinase Inhibitors. *Int. J. Mol. Sci.* **2009**, *10*, 2440−2475.
(59) Bhambhani, A.; Kumar, C. V. Enzyme−Inorganic Nanoporous Materials: Differential Scanning Calorimetric Studies and Protein Stability. *Microporous Mesoporous Mater.* **2008**, *109*, 223−232.
(60) Murphy, L. R.; Matubayasi, N.; Payne, V. A.; Levy, R. M. Protein Hydration and Unfolding—Insights from Experimental Partial Specific Volumes and Unfolded Protein Models. *Folding Des.* **1998**, *3*, 105−118.